phys. stat. sol. (a) **70**, 433 (1982)

Subject classification: 10.2; 22.5.2

Institut für Metallphysik der Universität Göttingen[1])

Slip on {100} Planes in LiF

By

Z. G. Liu and W. Skrotzki

Etching and slip line observations show that LiF single crystals compressed along ⟨111⟩ deform by slip on {100} planes. The temperature and strain rate dependence of the critical resolved shear stress as well as the activation volumes and activation enthalpies are consistent with a Peierls mechanism as rate controlling process below 450 K. An estimate of the Peierls stress yields $\tau_p^{\{100\}} = (380 \pm 30)$ MPa, which is about 20 times higher than that for primary slip on {110} planes.

Ätz- und Gleitlinienbeobachtungen zeigen, daß LiF-Einkristalle bei Druck in ⟨111⟩-Richtung sich auf {100}-Ebenen verformen. Die Abhängigkeit der kritischen Schubspannung von Temperatur und Verformungsgeschwindigkeit als auch Aktivierungsvolumen und Aktivierungsenthalpien sind verträglich mit einem Peierlsmechanismus als dem geschwindigkeitsbestimmenden Prozeß unterhalb 450 K. Eine Abschätzung der Peierlsspannung ergibt $\tau_p^{\{100\}} = (380 \pm 30)$ MPa, einen etwa 20 mal höheren Wert als für primäre Gleitung auf {110}-Ebenen.

1. Introduction

Information in the literature about secondary slip on {100} planes in LiF is very scarce. Gilman [1] reports cubic slip produced by torsion of ⟨100⟩ oriented crystals. However, his crystals were rather impure as indicated by an extremely high yield stress for {110} slip. Budworth and Pask [2] deformed ⟨111⟩ oriented crystals and assumed without proof {100} slip for their interpretation of the critical flow stress. Other publications about cubic slip in LiF are not known to us. Therefore, it seemed necessary to obtain more accurate and extended data on {100} slip in purer LiF crystals which are now available. This work continues investigations recently published on a series of ionic crystals [3 to 5] with the aim to find out the rate controlling mechanism determining the strong plastic anisotropy of these materials.

2. Experimental

The investigations have been carried out on LiF single crystals of different purities. The content of divalent impurities determined by atomic emission spectroscopy with inductively coupled plasma is given in Table 1 together with the room temperature critical resolved shear stresses (CRSS) for primary slip. ⟨111⟩ oriented specimens (dimensions $3.5 \times 3.5 \times 12$ mm^3) were cut by a diamond saw from a large block after embedding it in synthetic resin. Saw traces were removed by mechanical and chemical polishing. Deviations from ⟨111⟩ were not larger than 2° as checked by X-ray Laue photographs. All specimens have been annealed for 24 h at 973 K in evacuated quartz ampoules and then furnace-cooled (< 1 K/min). The density of grown-in dislocations (etch pits on {100}) was 10^4 to 10^5 cm^{-2}, the subgrain size about 1 to 2 mm. Suitable polishing and etching solutions for the {112} and {110} surfaces of the specimens

[1]) Hospitalstr. 12, D-3400 Göttingen, FRG.

Table 1
Crystal characteristics

LiF	Me^{2+}	$c_{Me^{2+}}$ (mol ppm)	$\tau_c^{\{110\}}$ (RT) (MPa)
I	Mg	< 14	0.74
	Ca	< 5	
	Sr	< 0.01	
	Ba	< 0.05	
II	Mg	< 17	5.5
	Ca	< 6	
	Sr	0.1	
	Ba	80	

were 100 ml destilled water with 3 mg $FeCl_3 \cdot 6\,H_2O$ and a mixture of 50 ml fluoboric acid, 50 ml formic acid, and 50 mg $FeCl_3 \cdot 6\,H_2O$, respectively. The polishing time was about 60 to 120 s for both planes while etching time was about 15 s for {112} and 100 to 150 s for {110}.

Dynamic compression tests were performed with an average initial strain rate $\dot{\varepsilon} \approx 5 \times 10^{-5}$/s. For axial loading a half steel ball was positioned on the upper sample end. Room temperature (RT) deformation was performed in air. For temperatures below RT and up to 500 K baths of isopentane and silicon oil, respectively, were used. Above 500 K the crystals were deformed in air in a furnace. The temperatures were kept constant to $\pm$ 2 K.

3. Results

3.1 Proof of {100} slip

⟨111⟩ oriented crystals are suitable for {100} slip because the Schmid factor for cubic slip is 0.47, while the Schmid factor for {110} slip is zero. To show that the deformation is really carried by the desired slip system the specimens have been etched just after the onset of deformation. Also slip line observations have been made after strains $\varepsilon \gtrapprox 1\%$.

At high temperatures ($T > 380$ K) and after strains $\varepsilon > 1\%$ the impure crystals show sharp slip lines on the {112} and {110} surfaces (Fig. 1). With decreasing temperature the slip lines become finer. Below 380 K no sharp slip lines can be detected by an optical microscope. At lower temperatures (320 K $< T <$ 450 K) traces of the activated {100} planes can be seen on the surfaces after etching (Fig. 2). Below 300 K small deviations of the specimen axis from the ⟨111⟩ orientation lead to additional {110} ⟨110⟩ slip because of the high plastic anisotropy (compare Fig. 4). Quenching crystals from high temperature ($\approx$ 873 K) in air on a metal plate produces high thermal stresses leading to cracks on {100} planes. These cracks can be used as an intrinsic reference system (see Fig. 1).

The slip behaviour of „pure" crystals differs from that of the impure ones. At the beginning of deformation only homogeneously distributed dislocations can here be observed after etching. Stronger deformation at high temperatures produces {100} ⟨110⟩ slip steps on the surface but they are not as sharp as for doped crystals (Fig. 3).

Generally it was observed that the slip mode changes with the Burgers vector of the dislocations relative to the surface. As has been already reported in [3, 6] the

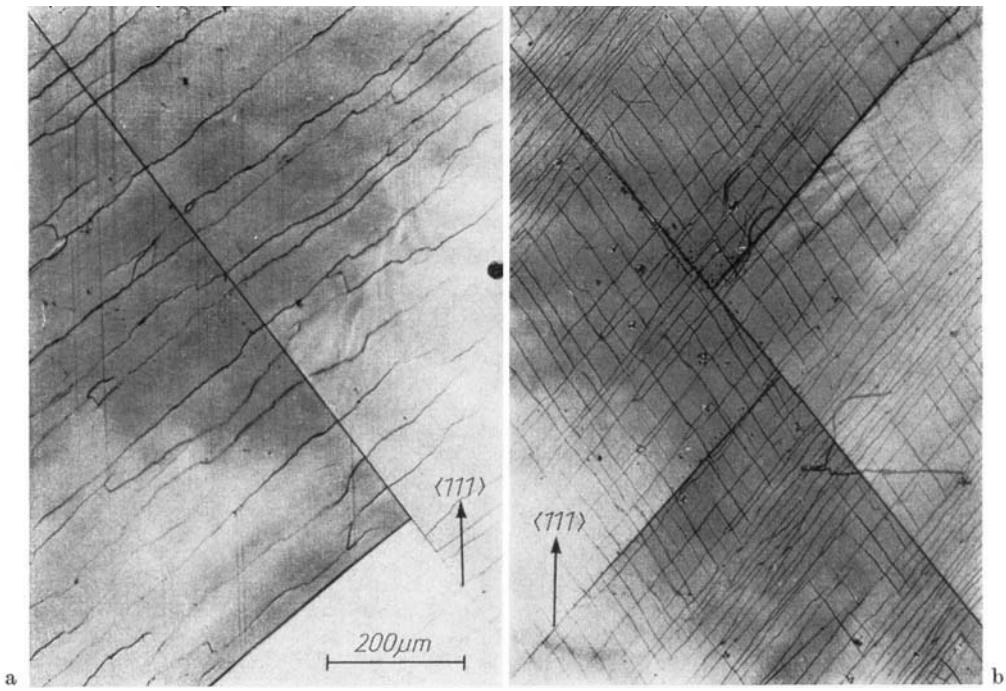

Fig. 1. Slip lines on the a) {110} and b) {112} surface planes of a ⟨111⟩ oriented LiF II crystal. Straight lines are cracks marking the traces of {100} planes ($T = 450$ K, $\varepsilon \approx 1.2\,\%$)

waviness of the slip bands increases with increasing screw character. The deviations of the slip lines from traces of {100} planes on the surface increases with decreasing temperature, i.e. with increasing plastic anisotropy.

3.2 Temperature and strain rate dependence of the CRSS

The CRSS for {100} slip has been determined from parabolical stress-strain curves as the proportional limit, the scatter being smaller than 8%. Its temperature dependence is shown in Fig. 4. Striking features are the following:

- There are temperatures $T_0^{\{110\}} \approx 40$ K and $T_0^{\{100\}} \approx 520$ K below which $\tau_c^{\{110\}}$ and $\tau_c^{\{100\}}$, respectively, increase strongly with decreasing temperature.
- $\tau_c^{\{110\}} \ll \tau_c^{\{100\}}$ below $T_0^{\{100\}}$.
- The CRSS of the impure crystals are larger than those of the pure ones in the temperature range 400 K $< T <$ 650 K. Above 650 K and below 400 K there is nearly no difference.
- The slope of the $\tau_c^{\{100\}}$ (T) curve becomes smaller below 300 K. Microscopical observations show that this correlates with the activation of {110} slip.

The strain rate dependence of the CRSS has been determined by strain rate changes during deformation of the same sample. Fig. 5 shows that ln $\dot{a}$ depends linearly on τ_c, the slope increasing with increasing temperature. The shear strain rate $\dot{a}$ is approximated by $\dot{\varepsilon}/0.47$.

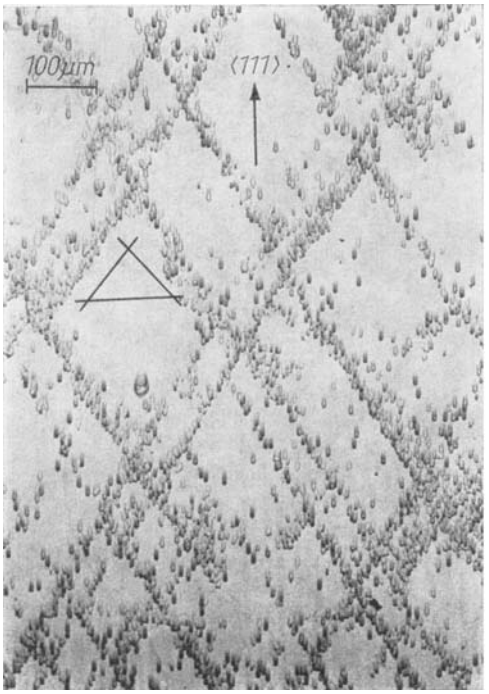

Fig. 2

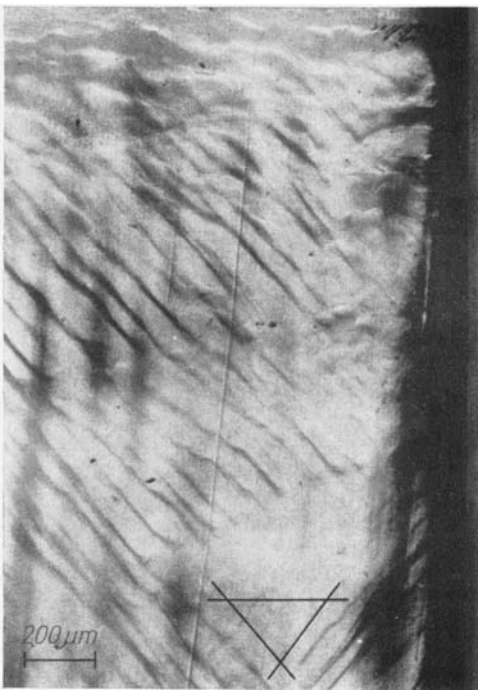

Fig. 3

Fig. 2. Slip bands on the etched {112} surface plane of a ⟨111⟩ oriented LiF crystal. Traces of the {100} planes are marked ($T = 380$ K, $\varepsilon \approx 0.1\%$)

Fig. 3. Slip lines on the {112} surface plane of a ⟨111⟩ oriented LiF I crystal. Traces of the {100} planes are marked ($T = 750$ K, $\varepsilon \approx 1.5\%$)

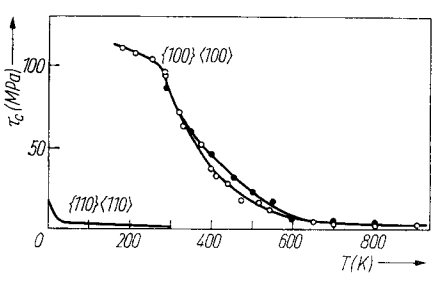

Fig. 4

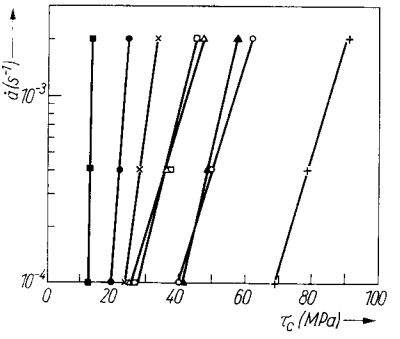

Fig. 5

Fig. 4. Temperature dependence of the CRSS. Curve for {110} slip refers to [7]

Fig. 5. Shear strain rate dependence of the CRSS. ■ $T = 552$, ● 480, × 450, □ 419, △ 390, ▲ 355, ○ 372, + 323 K

4. Analysis of the Results

The results are comparable to those obtained for other ionic crystals [3 to 5] and will be analysed in terms of the Peierls mechanism. For thermally activated processes the shear strain rate is usually described by an Arrhenius ansatz

$$\dot{a} = \dot{a}_0 \exp(-\Delta G/kT), \tag{1}$$

where $\dot{a}_0$ is a frequency factor and ΔG is the Gibbs free energy for dislocation movement. For particular forms of the Peierls potential the Gibbs free energy for double kink formation was evaluated by Celli et al [8]. According to them for a quasi-parabolic Peierls potential ΔG leads to

$$\Delta G = \Delta G_0 \left(1 - \frac{\tau}{\tau_p}\right)^2 \tag{2}$$

with

$$\Delta G_0 \approx a(ab\tau_p E_L)^{1/2} \tag{3}$$

(a distance between Peierls valleys, b magnitude of the Burgers vector, τ_p Peierls stress, E_L line tension).

At a constant strain rate a combination of (1) and (2) gives the stress-temperature relation as

$$\frac{\tau}{\tau_p} = 1 - \left(\frac{T}{T_0}\right)^{1/2} \tag{4}$$

with

$$T_0 = \frac{\Delta G_0}{k \ln \frac{\dot{a}_0}{\dot{a}}}. \tag{5}$$

Fig. 6 shows a plot of the temperature dependence of τ_c according to equation (4). The athermal component τ_μ resulting from long-range stresses of other dislocations has not been eliminated because $\tau_\mu \lessapprox \tau_c$ ($T > 520$ K) $\ll \tau_c$($T < 520$ K). The data can be fitted to a straight line below ≈ 450 K. Extrapolation to absolute zero yields $\tau_p = (380 \pm 30)$ MPa. Extrapolation to high temperatures yields $T_0 \approx 520$ K.

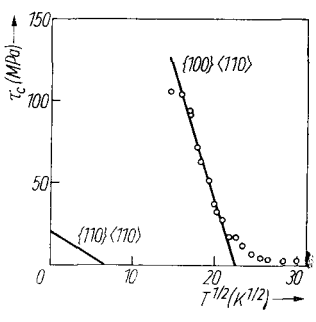

Fig. 6

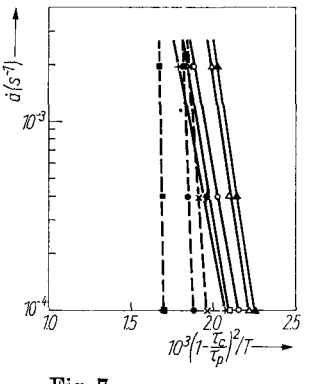

Fig. 7

Fig. 6. Temperature dependence of the CRSS presented in a τ_c vs. $T^{1/2}$ plot. Curve for {110} slip refers to [7]

Fig. 7. Plot of the shear strain rate versus $(1 - \tau_c/\tau_p)^2/T$, for $\tau_p = 380$ MPa. ■ $T = 552$, ● 480, × 450, □ 419, △ 390, ○ 372, ▲ 355, + 323 K

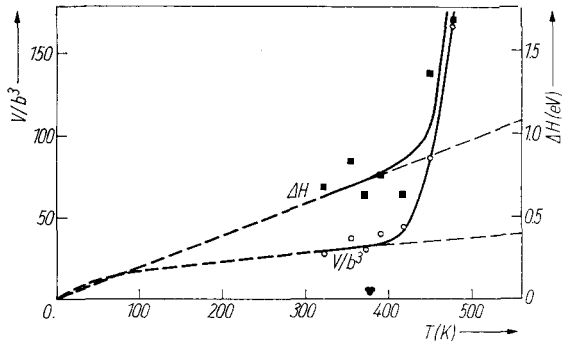

Fig. 8. Temperature dependence of the activation volume and the activation enthalpy. Dashed lines are calculated according to (8) and (9)

ΔG_0 and $\dot{a}_0$ can be determined from the strain rate dependence of the CRSS. Fig. 7 shows that a linear dependence between $\ln \dot{a}$ and $(1 - \tau_c/\tau_p)^2/T$ as predicted by (1) and (2) is obtained. The value of ΔG_0 determined from the slopes of the straight lines below 450 K (solid lines) is (1 ± 0.1) eV; $\dot{a}_0$ is found to be around $5 \times 10^{5\pm1}$ s^{-1}.

The line tension estimated from (3) using the obtained values for ΔG_0, τ_p, and $a = b$ is $E_L/\mu b^2 = 2.2$. This value coincides in the order of magnitude with Nabarro's estimate of 0.5.

A further confirmation of the Peierls mechanism is given by comparing the activation parameters estimated from experiment and theory. Fig. 8 shows the temperature dependence of the activation volume V and of the activation enthalpy ΔH determined from the strain rate and temperature dependence of the CRSS by the relations

$$V = kT\left(\frac{\partial \ln \dot{a}}{\partial \tau_c}\right)_T \tag{6}$$

and

$$\Delta H = -TV\left(\frac{\partial \tau_c}{\partial T}\right)_{\dot{a}}. \tag{7}$$

The agreement with the theoretical values estimated with the relations

$$V_{\text{theor}} = -\frac{\partial \Delta G}{\partial \tau_c} = \frac{2\Delta G_0}{\tau_p T_0^{1/2}} T^{1/2} \tag{8}$$

and

$$\Delta H_{\text{theor}} \approx \Delta G = \frac{\Delta G_0}{T_0} T \tag{9}$$

is good below 450 K.

The results of the analysis of the Peierls mechanism are presented in Table 2.

Table 2

Summary of the analysis. Values for {110} slip refer to [7]

	τ_p (MPa)	T_0 (K)	ΔG_0 (eV)	$\dot{a}_0$ (s^{-1})	$E_L/\mu b^2$
{100}	380 ± 30	520 ± 10	1 ± 0.1	$5 \times 10^{5\pm1}$	2.2
{110}	20	40	0.09 ± 0.01	$3 \times 10^{6\pm1}$	0.7 edge 2.0 screw

5. Discussion

5.1 Hardening mechanism

The analysis shows that the experimental results can be well explained in terms of the Peierls mechanism. The Peierls stress extrapolated here is only 20% higher than that estimated from Gilman's data [3, 5]. This agreement may be fortuitous because of the large quantitative differences. These may be caused by the high impurity content of Gilman's crystals which change the temperature dependence of $\tau_c^{\{100\}}$ (see Fig. 4).

An elastic model to calculate the Peierls stress has been developed by Peierls and Nabarro [9]. According to this theory τ_p is given by

$$\tau_p^{(\text{elast})} = \frac{2\mu}{1-\nu} \exp(-4\pi\xi/b) \tag{10}$$

with

$$\xi = \frac{s}{2(1-\nu)} \tag{11}$$

(2ξ dislocation width, s slip plane distance, ν Poisson ratio $= c_{12}/(c_{11}+c_{12}) = 0.25$). For non-dissociated dislocations (10) yields with $s^{\{100\}} = \sqrt{2}\, b/2$, $s^{\{110\}} = b/2$, $\mu^{\{100\}} = c_{44} = 6.49 \times 10^4$ MPa, $\mu\ \{110\} = (c_{11} - c_{12})/2 = 4.11 \times 10^4$ MPa: $\tau_p^{\{100\}}$ (elast) $= 463$ MPa, $\tau_p^{\{100\}}$(elast) $= 1662$ MPa.

Assuming dislocations to be dissociated on {110} as suggested by slip line observations [10, 6], then in the case of a high stacking fault energy the effective Peierls stress is $2\tau_p^{\{110\}}$ (for the partial dislocation) if $\xi \neq na$ (n integer) and smaller than $2\tau_p^{\{110\}}$ (for the partial dislocation) if $\xi \neq na$ [9]. $\tau_p^{\{110\}}$ (for the partial dislocation) is the stress obtained with (10) replacing b by the Burgers vector b_p of the partial dislocation. Using $b_p \approx b/2$ (10) yields $\tau_p^{\{110\}}$ (elast) $\lessapprox 50$ MPa.

A comparison with the experimental values (Table 2) shows that the Peierls-Nabarro theory gives the right plastic anisotropy in the case of dissociated {110} ⟨110⟩ dislocations but no quantitative agreement. The same holds for other alkali halides previously described [4].

According to a simple atomistic model of Gilman [11] $\tau_p^{\{100\}}$ is given by

$$\tau_p^{\{100\}}(\text{atomist}) \approx 0.035 \frac{e^2}{\varepsilon_0 b^4} \tag{12}$$

($\varepsilon_0 = 8.5$ static dielectric constant, e electron charge).

For LiF (12) yields $\tau_p^{\{100\}}$ (atomist) $= 150$ MPa. This value is smaller than that from experiment by a factor 2.5. Accurate atomistic calculations of the Peierls stresses of LiF are still missing.

Divalent impurities of about 100 ppm give rise to an increase of $\tau_c^{\{100\}}$ in the range $350\ \text{K} < T < 650\ \text{K}$. According to [3, 5] this hardening is due to the interaction of dislocations with impurity–vacancy dipoles or with aggregates of such obstacles. Above ≈ 500 K the impurity–vacancy dipoles begin to dissociate leading to less effective obstacles. As there is no difference between the CRSS of "pure" and impure crystals above 650 K it is concluded that at high temperatures τ_c is determined by dislocation–dislocation interactions requiring $\tau_c/\mu = \text{const}$. For {100} slip $\tau_c^{\{100\}}/\mu^{\{100\}} \approx 0.5 \times 10^{-4}$ above 650 K, for {110} slip $\tau_c^{\{110\}}/\mu^{\{110\}} \approx 0.2 \times 10^{-4}$ above 100 K. There is a stronger elastic interaction between dislocations on {100} than on {110} by a factor 2.5.

5.2 Slip mode

The slip bands of screw dislocations of the {100} ⟨110⟩ system are wavy in the whole investigated temperature range indicating easy cross slip. This observation is consistent with calculations of stacking fault energies which predict a much smaller dissociation on {100} than on {110} [12].

The preferred cross slip plane for {100} ⟨110⟩ dislocations is the {110} plane. This has been observed for other alkali halides [3] and there are indications that is true for LiF, too. The frequency of cross slip and the cross slip distance determines the deviations of the slip bands from traces of the {100} planes. With decreasing temperature these deviations become larger. This means that for non-dissociated screw dislocations thermal activation is not needed for cross slip and therefore this process becomes easier with increasing plastic anisotropy, i.e. with decreasing temperature. It is interesting to note that the deviations of slip bands from {100} traces are rather regular (Fig. 2): The slip bands appear to be symmetrical to the ⟨111⟩ axis.

Acknowledgements

Thanks are due to Prof. P. Haasen for helpful discussions and to the Deutsche Forschungsgemeinschaft (W.S.) and the government of The People's Republic of China (Z.G.L.) for support.

References

[1] J. J. Gilman, Acta metall. 7, 608 (1959).
[2] D. W. Budworth and J. A. Pask, J. Amer. Ceram. Soc. **46**, 560 (1963).
[3] W. Skrotzki, Ph. D. Thesis, Göttingen 1980.
[4] T. Suzuki, W. Skrotzki, and P. Haasen, phys. stat. sol. (b) **103**, 763 (1981).
[5] W. Skrotzki and P. Haasen, J. Physique **42**, C3-119 (1981).
[6] W. Skrotzki, G. Frommeyer, and P. Haasen, phys. stat. sol. (a) **66**, 219 (1981).
[7] T. Suzuki and H. Kim, J. Phys. Soc. Japan **39**, 1566 (1975).
[8] V. Celli, M. Kabler, T. Ninomya, and R. Thomson, Phys. Rev. **131**, 58 (1963).
[9] J. P. Hirth and J. Lothe, Theory of Crystal Dislocations, McGraw Hill, New York 1968 (p. 214).
[10] Z. G. Liu, Diploma Thesis, Göttingen 1981.
[11] J. J. Gilman, J. appl. Phys. **44**, 982 (1973).
[12] P. W. Tasker and T. J. Bullough, Phil. Mag. A **43**, 313 (1981).

(Received January 28, 1982)